Inorganic Chemistry

Article

pubs.acs.org/IC

Synthesis, Crystal Structure, and Magnetic Properties of Novel Intermetallic Compounds R_2Co_2SiC (R = Pr, Nd)

Sixuan Zhou,[†] Trinath Mishra,[†] Man Wang,[†] Michael Shatruk,[†] Huibo Cao,[‡] and Susan E. Latturner*[,†]

[†]Department of Chemistry and Biochemistry, Florida State University, Tallahassee, Florida 32306, United States

[‡]Quantum Condensed Matter Division, Oak Ridge National Laboratory, Oak Ridge, Tennessee 37831, United States

Supporting Information

ABSTRACT: The intermetallic compounds R_2Co_2SiC (R = Pr, Nd) were prepared from the reaction of silicon and carbon in either Pr/Co or Nd/Co eutectic flux. These phases crystallize with a new stuffed variant of the W_2CoB_2 structure type in orthorhombic space group *Immm* with unit cell parameters a = 3.978(4) Å, b = 6.094(5) Å, c = 8.903(8) Å (Z = 2; R_1 = 0.0302) for Nd_2Co_2SiC. Silicon, cobalt, and carbon atoms form two-dimensional flat sheets, which are separated by puckered layers of rare-earth cations. Magnetic susceptibility measurements indicate that the rare earth cations in both analogues order ferromagnetically at low temperature ($T_C \approx 12$ K for Nd_2Co_2SiC and $T_C \approx 20$ K for Pr_2Co_2SiC). Single-crystal neutron diffraction data for Nd_2Co_2SiC indicate that Nd moments initially align ferromagnetically along the c axis around ~12 K, but below 11 K, they tilt slightly away from the c axis, in the ac plane. Electronic structure calculations confirm the lack of spin polarization for Co 3d moments.

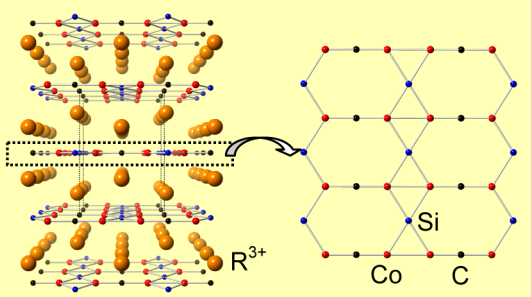

INTRODUCTION

Flux reactions in molten metal solvents are an excellent way to grow large crystals of complex intermetallic phases.[1] The solubility of many reactants in molten metal flux makes them active at temperatures well below their melting point. Common fluxes include low-melting main group metals such as Ga, Al, Sn, In, and Pb.[2,3] Rare earth metals and transition metals are not considered for use as fluxes due to their high melting points. However, when early rare earth metals (R = La, Ce, Pr, Nd) are combined with late first row transition metals (T = Co, Ni, Cu), eutectic mixtures with lowered melting points can form at specific ratios. For instance, a 64/36 atomic percent ratio of Nd/Co melts at 566 °C.[4]

We have found that R/T eutectic flux mixtures are excellent solvents for a variety of elements, including refractory metals and metalloids such as carbon and boron. New carbides and borides recently grown from R/T flux include $La_{14}Sn(MnC_6)_3$, $LaRu_2Al_2B$, $La_{21}Fe_8Sn_7C_{12}$, and $Ce_{33}Fe_{13}B_{18}C_{34}$.[5−8] The products are often rare earth rich, in accordance with the nature of the R/T solvent. The transition metals incorporated in these phases are capped by carbon or other light element atoms. The magnetic behavior is dependent on the extent of T−T bonding in the structure, with isolated transition metal sites or small transition metal clusters being nonmagnetic and larger clusters such as the Fe_4 and Fe_{13} clusters in $La_{21}Fe_8Sn_7C_{12}$ and $Ce_{33}Fe_{13}B_{18}C_{34}$ exhibiting a magnetic moment and ordering.[7,8]

Praseodymium- and neodymium-rich R/T fluxes are now being investigated for synthesis of intermetallics containing both a magnetic rare earth and a magnetic transition metal. Reactions of iron, silicon, and carbon were explored in Nd/Co and Pr/Co fluxes, resulting in formation of $R_2Co_{2-x}Fe_xSiC$ ($0 \le x < 0.3$). The reactivity of iron appears to have changed in going from the previously explored La- or Ce-rich fluxes to Pr- or Nd-rich melts; instead of preferential incorporation into products, iron now exhibits slight substitution onto cobalt sites. The title compounds have a new structure type, which features cobalt dimers capped by carbon and bridged by silicon, forming two-dimensional (2-D) sheets separated by layers of R^{3+} ions. Magnetic susceptibility measurements show that the magnetic moments of the rare earth ions in both analogues order ferromagnetically at low temperatures. Neutron diffraction studies for Nd_2Co_2SiC indicate that the Nd moments order in two steps, with a slight spin reorientation. Density of states calculations support the presence of a negligible cobalt moment, which does not exhibit spin polarization.

EXPERIMENTAL SECTION

Sample Preparation. The starting materials were stored and handled in an argon-filled glovebox. Neodymium chips (99.9%, Strem Chemicals), praseodymium chunks (99.9%, Alfa Aesar), cobalt slugs (99.95%, Alfa Aesar), powders of silicon (99.9%, Strem Chemicals), and acetylene carbon black (99.99%, Strem Chemicals) were used as received. The Nd/Co eutectic flux was made by arc melting Nd and Co (combined in a 64/36 mol ratio) under Zr-gettered argon atmosphere on a water-cooled copper hearth. Pellets were flipped and remelted several times to ensure homogeneity. Pr/Co flux was made in a similar manner, arc melting a combination of Pr and Co chunks in a 66/34 mol ratio. Reactants Si and C, mixed in 1:2 mmol ratio, were

Received: March 14, 2014
Published: June 5, 2014

   dx.doi.org/10.1021/ic5005984 | *Inorg. Chem.* 2014, 53, 6141−6148

sandwiched between layers of R/Co eutectic (broken into 1 mm^3 or smaller pieces; 0.75 g of the flux was below the powdered Si and C, and 0.75 g was above it) in an alumina crucible (i.d. 6 mm), which was placed in a silica tube. A second alumina crucible was filled with Fiberfrax and inverted above the reaction crucible to act as a filter during centrifugation. The silica tube was sealed under vacuum of 10^{-2} Torr. The ampule was heated to 950 °C in 3 h, held at this temperature for 12 h, and then cooled to 850 °C in 10 h. The reaction mixtures were subsequently annealed for 48 h at 850 °C and then cooled to 700 °C in 84 h. At 700 °C the ampule was removed from the furnace, quickly inverted, and centrifuged to decant the molten flux. Traces of residual flux were found on some samples; these were removed either by leaving the samples in air to preferentially oxidize the flux coating or by placing the crystals in hexane and scraping off surface layers.

To explore the phase width, reactivity of iron in Nd/Co flux, and magnetic behavior of iron-substituted $Nd_2Co_{2-x}Fe_xSiC$ phases, Nd/Co flux reactions were carried out with varying amounts of iron added as a reactant. As described above, Nd/Co eutectic flux was prepared, and 1.5 g of it was added to Si, C, and Fe powders combined in a 1:2:*X* mmol ratio, where the iron content *X* was varied from 0.20 to 1 mmol.

Stoichiometric syntheses of Nd_2Co_2SiC were attempted using reactants Nd, Co, Si, and C in a 2:2:1:1 mmol ratio. Reactions carried out in alumina crucibles sealed in silica tubes and heated to a temperature of 950 °C (similar to the procedure for the flux reactions) failed to produce Nd_2Co_2SiC, yielding NdCoSi instead. However, arc melting reactions proved more successful. Nd chunks, Co slugs, pieces of silicon wafer, and pieces of graphite crucible were combined in a 2:2:1:1 mmol ratio and arc-melted under argon. The resulting reaction pellet was flipped and arc-melted several times to ensure homogeneity. Powder X-ray diffraction data showed Nd_2Co_2SiC as the product, although a small number of extra weak diffraction peaks indicated formation of minor impurity phases, which could not be identified.

Elemental Analysis. Semiquantitative elemental analysis was performed with energy-dispersive X-ray spectroscopy (EDXS) on a JEOL 5900 scanning electron microscope (SEM) equipped with PGT Prism energy dispersion spectroscopy software. Flux-grown crystals were mounted onto an aluminum SEM holder with carbon tape, oriented with a flat face perpendicular to the electron beam, and analyzed using a 30 kV accelerating voltage and an accumulation time of 40 s. The carbon content was not determined due to the limitation of EDXS with light elements.

Single-Crystal X-ray Diffraction. Selected single crystals of each analogue were mounted on a glass fiber using epoxy. The single-crystal X-ray diffraction data were collected at room temperature on a Bruker AXS APEX2 CCD diffractometer equipped with a Mo-target X-ray tube (λ = 0.710 73 Å). The data sets were processed with the Bruker SAINT software.[9] An absorption correction was applied to the data with the SADABS program. The structure was solved in the centrosymmetric space group *Immm* (No. 71) and refined using the SHELXTL software package.[10] The data collection conditions and crystallographic parameters are shown in Tables 1 and 2. The standard axis setting for orthorhombic cells with no unique axis is used in this work (*a*, *b*, and *c* axes assigned according to axis length, with $a < b < c$). However, this structure is a stuffed variant of a previously reported structure type (W_2CoB_2), which is reported with a different arrangement of axes. An alternative unit cell setting of Nd_2Co_2SiC that is more directly comparable to W_2CoB_2 is described in Supporting Information (Table S1, Figure S1).

Single-Crystal Neutron Diffraction. To gain more insight into the magnetic ordering transition, a large single crystal of Nd_2Co_2SiC (0.7 mm × 0.5 mm × 3 mm) was studied by neutron diffraction at the HB-3A four-circle single-crystal diffractometer at the High Flux Isotope Reactor at Oak Ridge National Laboratory. Data were collected at 4, 25, and 250 K with neutron wavelength 1.5424 Å generated from a bent perfect Si-220 monochromator.[11] Differences in peak intensity were used to determine the magnetic structure at 4 K (below the ordering temperature of 11 K). The neutron diffraction data collection conditions and refined structural and magnetic parameters are shown in Supporting Information, Table S2. The intensities of several selected peaks were monitored as the temperature was increased from 4 to 20 K in 0.2 K increments (with 30 s dwell to stabilize at each temperature), counting for 1 min at each temperature, to observe the magnetic ordering temperature.

Table 1. Crystallographic Data Collection Parameters for R_2Co_2SiC

	Pr_2Co_2SiC	Nd_2Co_2SiC
crystal system	orthorhombic	
space group	*Immm* (No. 71)	
cell parameters (Å)	a = 4.003(1)	a = 3.978(4)
	b = 6.106(2)	b = 6.094(6)
	c = 8.989(3)	c = 8.903(8)
V (Å^3)	219.7(1)	215.8(3)
formula weight (g/mol)	439.8	446.4
Z	2	
calc. density (g/cm^3)	6.647	6.871
radiation	Mo Kα (λ = 0.710 71 Å)	
temperature (K)	296	
μ (mm^{-1})	29.257	31.271
$R_1/wR_2{}^a$ ($I > 2\sigma(I)$)	0.0220/0.0540	0.0302/0.0782
R_1/wR_2 (all data)	0.0237/0.0546	0.0305/0.0785

$^aR_1 = \sum||F_0| - |F_c||/\sum|F_0|$; $wR_2 = [\sum[w(F_0^2 - F_c^2)^2]/\sum[w(F_0^2)^2]]^{1/2}$

Table 2. Atom Positions and Thermal Parameters for Nd_2Co_2SiC

	Wyckoff Site	x	y	z	U_{eq}
Nd	4*j*	1/2	0	0.30941(7)	0.0080(5)
Co	4*h*	0	0.2949(3)	1/2	0.0080(6)
Si	2*a*	0	0	0	0.0085(10)
C	2*c*	1/2	1/2	0	0.013(4)

Magnetic Susceptibility Measurements. Magnetic susceptibility measurements were carried out on a Quantum Design SQUID Magnetic Property Measurement System. Crystals were selected and held between two strips of Kapton type, oriented with the crystallographic *a* axis (the longest physical dimension of the rod-shaped crystals is along the crystallographic *a* axis) either along the applied field or perpendicular to it. Temperature-dependent susceptibility data were collected between 1.8 and 300 K at various fields. Field-dependent data for the Nd_2Co_2SiC analogue were collected at several temperatures using fields up to 5 T; crystals were oriented with *a* axis either parallel to the applied field or perpendicular to the applied field. Field-dependent data for Pr_2Co_2SiC analogue were collected at 1.8 K using fields up to 7 T; crystals were oriented with *a* axis parallel to the applied field.

Electronic Structure Calculations. Density functional theory (DFT) band structure calculations were performed with a full potential all-electron local orbital code FPLO (version fplo7.00–28) within the local spin density approximation (LSDA) including spin–orbit coupling.[12] The Perdew–Wang parametrization of the exchange-correlation potentials was employed.[13] The strong Coulomb repulsion in the Nd 4f orbitals was treated on a mean-field level using the LSDA +*U* approximation in the atomic-limit double counting scheme.[14] The scalar-relativistic Dirac equation was solved self-consistently. The results presented below use the LSDA+*U* method[15] in the rotationally invariant form.[16] As a representative value, U = 8 eV was chosen. A variation of *U* between 7 and 9 eV did not influence significantly the relevant density of states (DOS) and energy. Structural parameters (unit cell dimensions and atomic coordinates) were taken from the room-temperature crystal structure of Nd_2Co_2SiC. The nonpolarized and spin-polarized DOS were calculated after convergence of the total energy on a dense *k* mesh with 32 × 32 × 32 points in the irreducible wedge of the Brillouin zone. The self-consistent criterion for the total energy conversion was equal to 10^{-8} Ha (≈ 2.72 × 10^{-7} eV).

dx.doi.org/10.1021/ic5005984 | *Inorg. Chem.* 2014, 53, 6141–6148

Crystal orbital Hamilton population analyses were obtained using tight binding calculations performed according to the linear muffin-tin orbital (LMTO) method in the atomic sphere approximation (ASA).[17−19] No additional empty spheres were necessary beyond those described automatically, subject to a 16% overlap restriction between atom-centered spheres. Their radii were Nd = 2.04 Å, Co = 1.16 Å, Si = 1.67 Å, and C = 1.00 Å. The basis sets of Nd 6s, 5d, (6p); Co 4s, 4p, 3d; Si 3s, 3p, (3d); and C 2s, 2p, (3d) (downfolded orbitals in parentheses) were employed. Nd 4f electrons were considered as core. The band structure was sampled at 12 × 12 × 12 *k* points in the irreducible wedge of the Brillouin zone.

RESULTS AND DISCUSSION

Synthesis. R_2Co_2SiC (R = Pr or Nd) grows from reactions of silicon and carbon in R/Co flux as silver, faceted rectangular rods, up to ∼5 mm in length. The reaction yield is about 60% based on silicon. X-ray powder diffraction studies indicate that the products of flux reactions are predominantly single phase with very small amounts (10% or less, see Supporting Information, Figure S2) of byproducts such as Nd_4Co_3. The crystalline samples are very stable in dry air for months, but are reactive toward water. Polycrystalline samples of Nd_2Co_2SiC can be synthesized by arc melting a stoichiometric ratio of Nd/Co/Si/C (2:2:1:1 mmol ratio); this yields the Nd_2Co_2SiC phase as the major product, see Supporting Information, Figure S3. Annealing of the arc-melted pellet may improve the crystallinity and potentially eliminate traces of impurities in the product, but this was not explored. Attempts to make R_2Co_2SiC with other rare earth metals such as La or Ce (either by arc melting stoichiometric mixtures, or from flux reactions of Si and C in La/Co or Ce/Co eutectics) were not successful.

It is notable that this phase was initially discovered from reactions of iron, silicon, and carbon in Nd/Co flux, carried out in an effort to make Nd/Fe/Si/C phases. Our previous work on R/Co and R/Ni fluxes (with R = La, Ce) indicated that if iron is added as a reactant, it is preferentially incorporated into products. For instance, reactions of Fe, Ge, and C in La/Ni flux produce $La_{21}Fe_8Ge_7C_{12}$ with no nickel incorporation.[7] Likewise, reactions of Fe, B, and C in Ce/Co flux produce $Ce_{33}Fe_{14}B_{25}C_{34}$.[8] However, this reactivity trend seems to change when heavier rare earths are used. If iron is present in the Nd/Co/(Fe)/Si/C reactions, Nd/Fe/Si/C phases are not formed. Instead, trace amounts of iron are incorporated into the Nd_2Co_2SiC phase, substituting on the cobalt sites. Incorporation of iron is confirmed by SEM/EDS data and by small changes in the unit cell parameters as Co is replaced by Fe (see Supporting Information, Figure S2).

Structure. R_2Co_2SiC phases exhibit a remarkably simple stoichiometry and a new structure type in orthorhombic space group *Immm* (Pearson symbol *oI*12). Given the interest in compounds containing rare earth metals, magnetic first row transition metals, and light metalloids (such as RNi_2B_2C superconductors and the strong magnetic phase $Nd_2Fe_{14}B$),[20,21] it is surprising that no compounds with the Nd_2Co_2SiC structure type have been reported so far. Other known ordered quaternary phases containing silicon and carbon combined with a rare earth and a transition metal include $Dy_2Fe_2Si_2C$, $DyFe_2SiC$, and $CeCr_2Si_2C$, and their analogues.[22−24] These phases (and the title phase) feature fully occupied carbon sites; this distinguishes them from disordered carbides such as $Nd_2Fe_{17-x}Si_xC_y$ and $NdCo_9Si_2C_{0.6}$ in which carbon partially occupies interstitial sites.[25,26]

The structure of Nd_2Co_2SiC (shown in Figure 1) is composed of puckered layers of Nd^{3+} ions sandwiched between

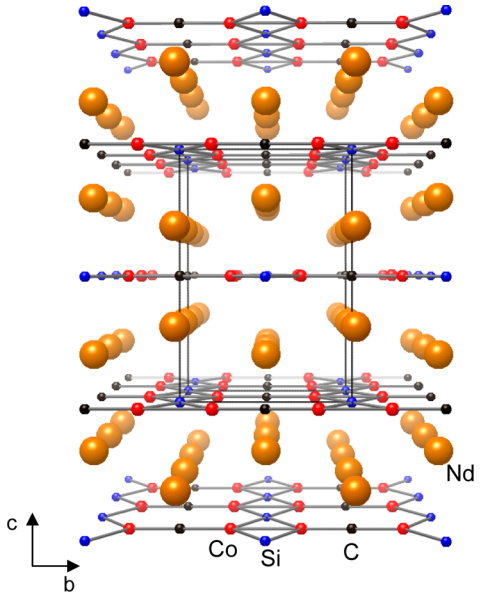

Figure 1. Nd_2Co_2SiC structure, viewed down the *a* axis. Large orange spheres are Nd; smaller blue, red, and black spheres represent Si, Co, and C atoms, respectively.

2-D Co/Si/C anionic sheets, which are stacked along the *c* axis of the unit cell. The two nonmetal elements are separated; instead of Si−C bonding, the silicon is bonded to four neighboring cobalt sites, with Nd ions at longer distances. The Co−Si distance of 2.349(2) Å is similar to that seen in $NdCo_9Si_2C_{0.6}$ (2.37 Å).[26] The carbon is bonded to two cobalt atoms with a short Co−C bond length of 1.797(2) Å, and four neighboring Nd^{3+} ions resulting in overall octahedral coordination. Octahedral coordination is also seen for carbon in $Dy_2Fe_2Si_2C$ (coordinated to two Fe and four Dy), $CeCr_2Si_2C$ (four Cr, two Ce), and $NdCo_9Si_2C_{0.6}$ (four Co, two Nd).[22,24,26] The R_2Co_2SiC structure is a stuffed variant of the W_2CoB_2 structure type (and the isopointal K_2PtS_2 type), with the rare earth ion on the W site, cobalt on the B site, and silicon on the Co site of W_2CoB_2.[27] The carbon atom occupies a new (stuffed) position in the structure. A comparison between the structure types can be found in the Supporting Information (Figure S1).

Positioning of the cobalt atoms and Nd^{3+} ions are of particular interest, given the potential magnetic behavior of these atoms. The cobalt site is bonded to a symmetry equivalent at a short distance of 2.500(4) Å, within the 2.44−2.63 Å range of Co−Co distances in $NdCo_9Si_2C_{0.6}$. The Co−Co dimers are bridged by two Si atoms, forming chains of these diamond-shaped units running in the *a* axis direction. The *a* axis corresponds to the longest physical dimension of the rod-shaped crystals, indicating crystal growth is most rapid in this direction. The bridged Co−Co dimers are terminated by carbon atoms, resulting in one-dimensional (1-D) infinite linear chains formed by Co−Co dimers and C atoms running along the *b* axis direction (see Figure 2). The Nd ions comprise a puckered sheet with Nd−Nd distances of 3.789(3) and 3.978(3) Å within this layer. However, a shorter Nd−Nd distance of 3.393(3) Å is found across the anionic Co/Si/C sheet. These three different distances may lead to complex magnetic behavior arising from the Nd sublattice alone, as well as from possible Co−Co and Co−Nd coupling interactions.

dx.doi.org/10.1021/ic5005984 | *Inorg. Chem.* 2014, 53, 6141−6148

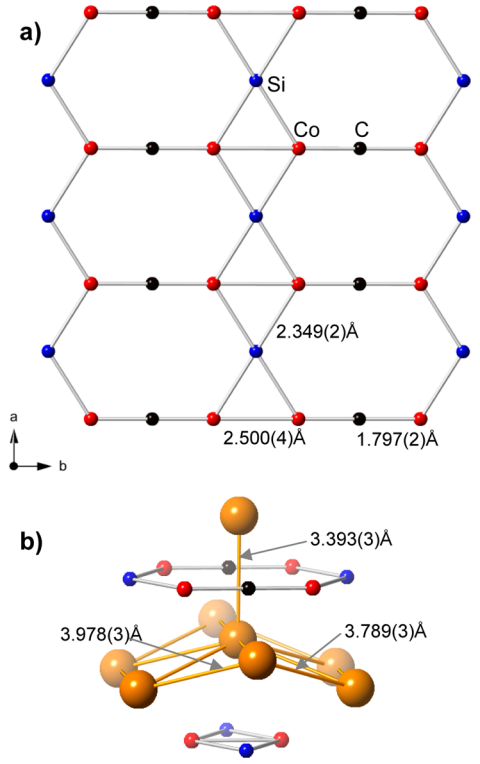

Figure 2. (a) The Co/Si/C sheet in Nd_2Co_2SiC, viewed down the *c* axis. (b) Coordination environment around the Nd site, with Nd–Nd distances below 4 Å indicated by yellow lines.

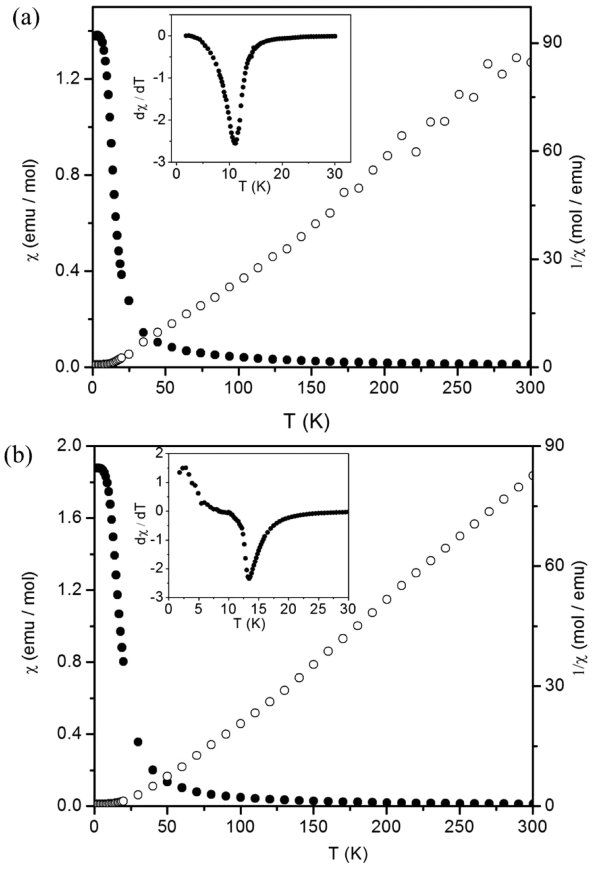

Figure 3. Temperature dependence of magnetic susceptibility data (filled circles) and inverse susceptibility data (empty circles) for Nd_2Co_2SiC measured with an applied field of 1 T. (a) Crystal aligned with *a* axis parallel to applied field. (b) Crystal aligned with *a* axis perpendicular to applied field. The Curie temperatures have been calculated from the derivative plot of χ vs *T* data measured at 0.1 T field (insets).

Magnetic Behavior. Flux growth of large crystals of Nd_2Co_2SiC allowed for susceptibility measurements in different orientations (with the long axis of the crystal—corresponding to the crystallographic *a* axis—parallel or perpendicular to applied field; see Figure 3). Initial measurements were hindered by an impurity (Figure S4, Supporting Information). These data showed a clear ferromagnetic ordering at 12 K, but also indicated a small but distinct increase in the susceptibility at 200 K. The samples were grown from Nd/Co eutectic, and traces of the flux may have adhered to the crystal, forming Nd_4Co_3 upon solidification. This phase (which was initially reported in the literature as $Nd_2Co_{1.7}$) is known to undergo ferromagnetic ordering at 202 K.[28] At high temperatures, Nd_2Co_2SiC is paramagnetic; data above 200 K can be fitted with the Curie–Weiss law to indicate a moment per Nd^{3+} ion of 5.2 μ_B. This is significantly higher than the theoretical value for Nd^{3+} (3.28 μ_B), due to the surface contamination.

Subsequent measurements on a Nd_2Co_2SiC crystal with this impurity removed by manually scraping off surface layers under hexane did not show the feature at 200 K; only the low temperature ferromagnetic ordering is seen (Figure 3). The magnetic susceptibility measurements were carried out with an applied field of 1 T. The crystal (0.5 mm × 1 mm × 4 mm) was oriented with crystallographic *a* axis either parallel to the applied field (Figure 3a) or perpendicular to the applied field (Figure 3b). The Curie–Weiss fit of the data well above the ordering temperature (data from 100–300 K) yields an effective moment of 2.47(1) μ_B per Nd atom and a Weiss constant of θ = 29(1) K for *a* axis alignment parallel to the field; a moment of 2.51(1) μ_B per Nd atom and a Weiss constant of θ = 37(1) K is achieved with *a* axis perpendicular to the field. The observed ferromagnetic ordering temperatures (parallel alignment T_C = 11.2(1) K and perpendicular alignment T_C = 13.4(1) K) were determined from the derivative plots of additional χ vs *T* measurements at 0.1 T field; see the insets in Figure 3.

The observed values for μ_{eff}, θ, and T_C are slightly larger when the crystal is aligned with the *a* axis perpendicular to field compared to when this axis is parallel to the field. This indicates that the Nd^{3+} magnetic moments tend to align perpendicular to the *a* axis. Indeed, as will be demonstrated below by neutron diffraction data, the Nd moments order ferromagnetically along the *c* axis at 13.4(1) K and then reorient slightly away from this direction on further cooling to 11.2(1) K. Field-dependent magnetization data collected at various temperatures are shown in Figure 4. Complete ferromagnetic saturation is not seen below T_C for either orientation; at 1.8 K and high applied fields, the Nd moments approach maximum values of 2.0 μ_B (perpendicular to the *a* axis) and 1.7 μ_B (parallel to the *a* axis). In addition to a larger moment, the magnetization in the direction perpendicular to the *a* axis also shows a larger hysteresis and more closely approaches saturation. This is in agreement with the *c* axis being an easy magnetization direction. A two-step ordering mechanism is suggested by the magnetization data at various temperatures. When the crystal is aligned with *a* axis parallel to the field, the field dependence data at 11 and 12 K are very similar, but the 10 K data exhibits a

dx.doi.org/10.1021/ic5005984 | Inorg. Chem. 2014, 53, 6141–6148

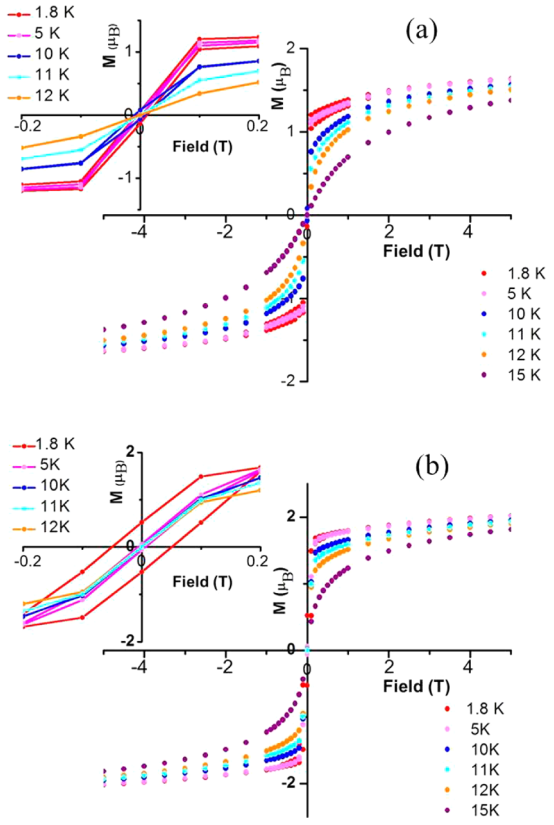

Figure 4. Magnetization data for Nd_2Co_2SiC at various temperatures spanning the ferromagnetic transition. (a) Crystal aligned with *a* axis parallel to applied field. (b) Crystal aligned with *a* axis perpendicular to applied field. Insets highlight the low-field region for each orientation.

slight hysteresis. This is not seen when the crystal is aligned in the other direction; the 10, 11, and 12 K curves are nearly identical and exhibit no hysteresis. This supports the idea that the Nd moments initially align ferromagnetically along the *c* axis around 13 K, but below 11 K, tilt slightly in the *a* axis direction, in the *ac* plane.

Single-crystal neutron diffraction data were collected on Nd_2Co_2SiC to clarify the nature of the ferromagnetic ordering and determine the contributions of Nd and Co to the magnetic behavior. Data sets were collected at 4, 25, and 250 K to observe the changes in peak intensity due to magnetic contributions. No significant difference was seen between the 25 and 250 K data sets, indicating that no magnetic ordering occurs in this temperature range. The magnetic component of the diffraction peaks at 4 K (below T_C) was isolated by subtracting the nuclear contribution determined from the 25 K data set, yielding 38 extracted magnetic peaks above the 2σ cutoff, which were used to determine the magnetic structure. The resulting model is shown in Figure 5. The neodymium ions have a magnetic moment of 2.07(2) μ_B and are nearly aligned with the *c* axis, in agreement with the magnetic susceptibility data. There is a slight canting at an angle $\varphi = 30(1)^\circ$ to the *c* axis, in the *ac* plane. The magnetic moment is lower that the theoretical value of 3.28 μ_B expected for Nd^{3+} ions; low Nd moments were also obtained from the magnetic susceptibility and magnetization data. The reduced moment is likely due to crystal electric field (CEF) effects, which will split the $^4I_{9/2}$ ground state at low temperatures. Similar effects have been reported for neodymium metal itself (Nd moment of 2.3 μ_B at

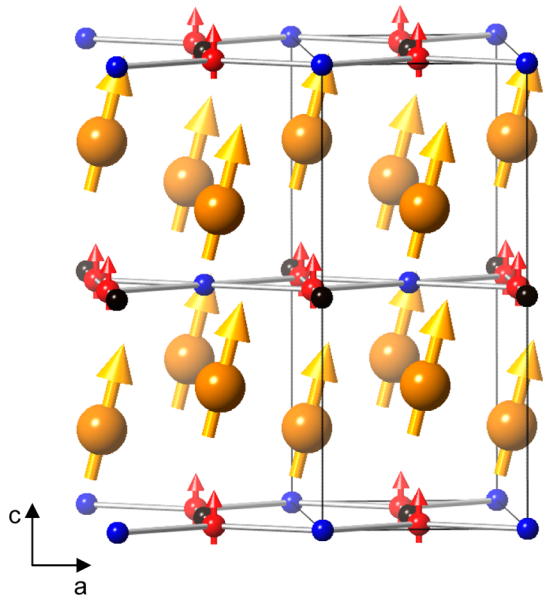

Figure 5. Magnetic structure of Nd_2Co_2SiC determined by neutron diffraction data collected on a single crystal at 4 K.

1.8 K)[29] and many other Nd-containing intermetallics.[30] The cobalt atoms have a very small magnetic moment of 0.21(5) μ_B, aligned along the *c* axis. This cobalt moment is almost negligible, but incorporating it into the final model improved the overall fit. The presence of cobalt moments could not be confirmed by magnetic susceptibility measurements or theoretical calculations, which indicate nearly zero spin polarization for the Co sublattice (vide infra). Possibly, the cobalt moments are induced by the ordering of the Nd moments below T_C.

The intensities of selected peaks were monitored as the temperature was raised from 4 to 20 K in 0.2 K increments. A clear increase in intensity is seen at the Curie temperature; see Figure 6. It is notable that the (002) diffraction peak indicates a T_C of 11 K, whereas the (020) and (200) peaks show an intensity increase at 12.5 K. This is further indication that the magnetic structure orders at 12.5 K with Nd moments aligned along the *c* axis, and then the moments reorient away from the *c* axis, as indicated by the increase in intensity of the (002) peak upon cooling to 11 K. The fact that magnetic peaks are seen along the (002), (020), and (200) axes below 11 K indicates the magnetic vector is not collinear with any of these axes.

The magnetic susceptibility data for Pr_2Co_2SiC are shown in Figure 7a. The low-temperature ferromagnetic transition is again apparent, with the Pr^{3+} moments ordering at $T_c = 20(1)$ K. No higher temperature transition is seen. Traces of Pr_4Co_3 might be expected to form from any flux residue on the crystal; this phase has a ferromagnetic transition at 142 K.[28] No anomaly is seen at this temperature in the data for Pr_2Co_2SiC, indicating this crystal has no contamination. The inverse susceptibility data above 50 K is linear and can be fit to the Curie–Weiss law, yielding an effective magnetic moment of 2.76(1) μ_B/Pr atom and Weiss constant $\theta = 30(1)$ K. The effective magnetic moment is lower than the theoretical value of 3.58 μ_B for a free Pr^{3+} ion, similar to the situation observed for the Nd-containing analogue. The positive Weiss constant θ is indicative of ferromagnetic interactions. The magnetization data for Pr_2Co_2SiC at 1.8 K exhibit slight hysteresis, with a saturation moment of 2.4(1) μ_B/Pr ion, remanent magnet-

dx.doi.org/10.1021/ic5005984 | Inorg. Chem. 2014, 53, 6141–6148

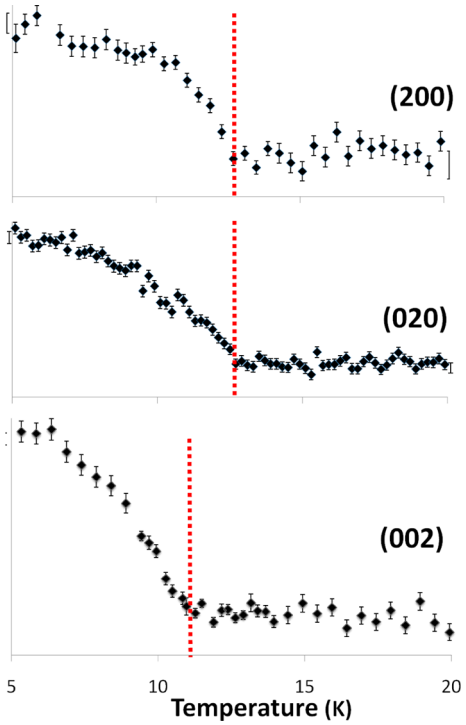

Figure 6. Temperature dependence of single-crystal neutron diffraction peak intensity for the (200), (020), and (002) diffraction peaks of Nd_2Co_2SiC; ordering temperatures indicated by red line.

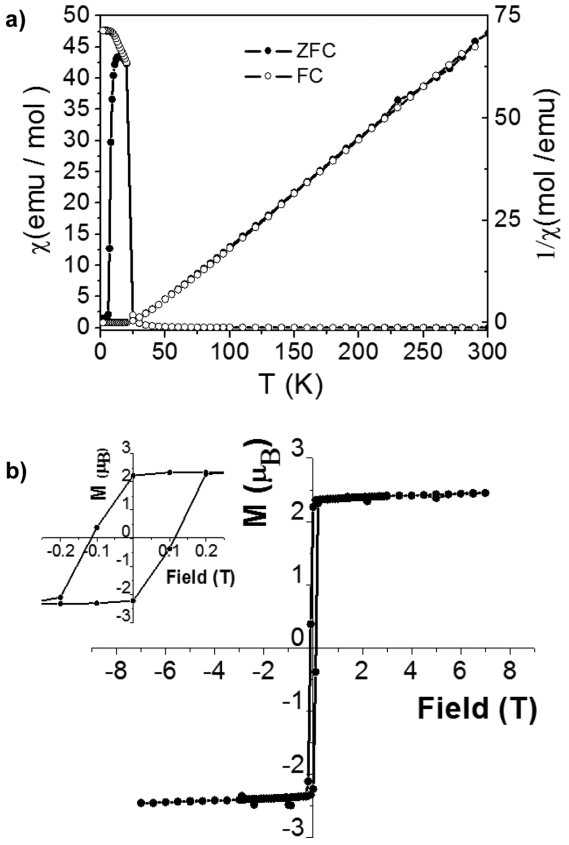

Figure 7. Magnetic susceptibility data for Pr_2Co_2SiC. (a) Temperature-dependence data measured with an applied field of 0.01 T, with *a* axis of crystal aligned parallel to applied field. (b) Magnetization data collected at 1.8 K, with *a* axis of the crystal aligned parallel to the applied field.

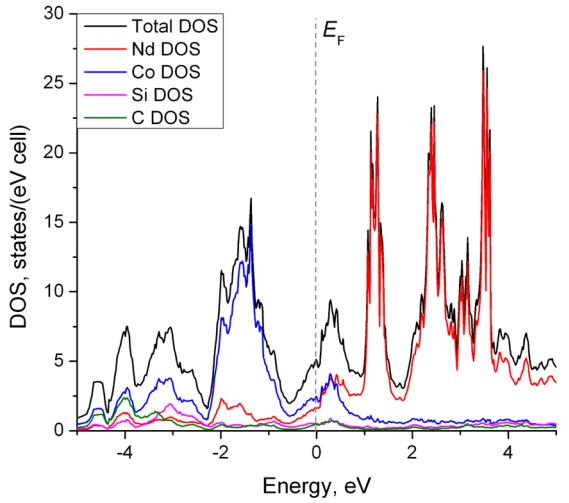

Figure 8. Densities-of-states (DOS) data calculated for Nd_2Co_2SiC.

ization of 2.2(1) μ_B/Pr ion, and a coercive field of 0.114 T. The susceptibility data in Figure 7a were collected at a smaller field (0.01T) and, therefore, exhibit differences in the field-cooled versus zero-field-cooled data below T_C due to domain wall motion. Pr_2Co_2SiC is a slightly harder ferromagnet than the neodymium analogue, due to the larger single-ion magnetic anisotropy of Pr^{3+}.

Electronic Structure Calculations. Both nonmagnetic and spin-polarized band structure calculations were performed for R_2Co_2SiC. The nonmagnetic DOS plot is shown in Figure 8. The nonzero DOS at the Fermi energy indicates that Nd_2Co_2SiC is metallic. Nd 5d states have the main contribution to the DOS above E_F, whereas orbitals from C, Si, and Co are dominant below the E_F. The data reveal only a small contribution from the Co 3d electrons at the Fermi level, $N \approx 0.6$ states/eV per Co atom. Assuming that the Co−Co magnetic exchange coupling in this compound does not exceed the values reported for cobalt metal ($J \approx 0.49$ eV),[12] one can easily see that the Stoner criterion of itinerant ferromagnetism, $JN(E_F) > 1$, is not satisfied for R_2Co_2SiC. This notion is supported by spin-polarized calculations, which indicate a magnetic moment of 3.2 μ_B per Nd atom and a negligibly small moment of only 0.027 μ_B per Co atom (Figure S5, Supporting Information). Note that the calculations did not take into account possible CEF effects, and, thus, the obtained value for the Nd magnetic moment, while in agreement with the theoretically expected value of 3.28 μ_B, does not agree with the experimental moments determined from the magnetic and neutron diffraction data. Nevertheless, the negligible spin polarization of the Co sublattice is in agreement with the experimental findings.

The crystal orbital Hamilton populations (COHP) for Nd_2Co_2SiC were calculated with the LMTO method and are illustrated in Figure 9. Observed bond length ranges and corresponding integrated COHP (ICOHP) values are listed in Table 3. In general, the larger ICOHP values correspond to shorter bonds and presumably stronger interactions. The interactions of the Co atoms with C and Si yield the two largest ICOHP values per contact (5.74 and 2.09 eV/bond) followed by a small value 0.82 eV/bond for the Co−Co bonds within the 2-D Co/Si/C anionic sheets (Figure 2). Co−C interactions (1.797 Å) within 1-D infinite linear chains formed

dx.doi.org/10.1021/ic5005984 | Inorg. Chem. 2014, 53, 6141−6148

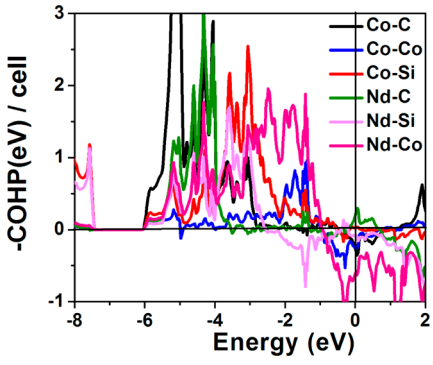

Figure 9. COHP curves for Nd_2Co_2SiC: Co−C (black), Co−Co (blue), Co−Si (red), Nd−C (green), Nd−Si (magenta), Nd−Co (pink). Nd−Nd data are not significant.

Table 3. Bond Lengths and ICOHP Values for Nd_2Co_2SiC

bond	length (Å)	-ICOHP (eV/per bond)	*n*/ cell	-ICOHP (eV/cell)	%
Co−C	1.797(2)	5.74	6	34.44	31.3
Co−Si	2.349(2)	2.09	8	16.72	15.2
Co−Co	2.500(4)	0.82	3	2.46	2.2
Nd−C	2.614(2)	1.55	12	18.6	16.9
Nd−Si	3.398(2)	0.58	24	13.92	12.6
Nd−Co	3.025(2), 3.173(2)	0.65	28	18.2	16.5
Nd−Nd	3.394(3), 3.789(2)	0.48	12	5.76	5.2

by Co and C atoms constitute 31.3% of the total ICOHP per cell. The interactions of the Nd cations with Co, Si, and C atoms present in the 2-D Co/Si/C anionic sheets comprise 46% of the total ICOHP per cell; the bonding along the stacking direction is quite strong. Because of the filling of the Co 3d orbitals, antibonding states start to appear below E_F and extend to the conduction band. The Co−Co, Nd−Co, and Nd−Si interactions are both bonding/antibonding within the valence band, whereas Co−C, Co−Si, and Nd−C interactions are mainly bonding and, therefore, contribute to the stability of the Nd_2Co_2SiC structure. There is great theoretical interest in Co_2 dimers, which are predicted to have large magnetic anisotropy energies.[31] Unfortunately, the very small Co−Co ICOHP and the much stronger interactions of the cobalt atoms with surrounding heteroatoms indicate that the Co−Co unit in Nd_2Co_2SiC is not behaving as a dimer; this is in agreement with its nonmagnetic nature.

CONCLUSION

Metal fluxes composed of R/Co mixtures are excellent solvents for refractory elements; reactions of carbon and silicon in these mixtures resulted in the formation of novel ferromagnetic intermetallic compounds R_2Co_2SiC (R = Pr, Nd). While the new structure type features Co−Co bonding, the magnetic behavior stems from the rare earth ions; the cobalt atoms have a negligible magnetic moment. This is confirmed by neutron diffraction data and magnetic susceptibility measurements. Electronic structure calculations also support this, showing few cobalt d-states at the Fermi level and very weak Co−Co interactions in the COHP. Further exploration is needed to find intermetallic phases containing strongly bonded Co dimer species, or possibly larger Co_n clusters, which will have strong magnetic moments on the cobalt atoms. These might exhibit magnetic coupling to each other and to the rare earth ions, which may result in unusual magnetic phenomena such as multiple ordering transitions or spin glass behavior.

ASSOCIATED CONTENT

Supporting Information

Comparison of Nd_2Co_2SiC and W_2CoB_2 structure types. Neutron diffraction refinement parameters for Nd_2Co_2SiC at 4 K and goodness-of-fit plot for magnetic structure characterization. Powder diffraction patterns of arc-melted Nd_2Co_2SiC and flux grown $Nd_2Co_{2-x}Fe_xSiC$ with varying amounts of iron added. Magnetic susceptibility data for Nd_2Co_2SiC crystals. Spin-polarized partial DOS plot for cobalt in Nd_2Co_2SiC. Single-crystal X-ray crystallographic information files (CIF) for both investigated compounds. This material is available free of charge via the Internet at http://pubs.acs.org.

AUTHOR INFORMATION

Corresponding Author

*E-mail: latturner@chem.fsu.edu.

Notes

The authors declare no competing financial interest.

ACKNOWLEDGMENTS

This research was supported by funding from the National Science Foundation (Division of Materials Research) through Grant No. DMR-11-06150 to S.E.L. and partially through Grant No. DMR-09-55353 to M.S. This work made use of the SEM Facilities of the FSU Physics Department. The research at ORNL High Flux Isotope Reactor was sponsored by the Scientific User Facilities Division, Office of Basic Energy Sciences, U.S. Department of Energy.

REFERENCES

(1) Kanatzidis, M. G.; Pöttgen, R.; Jeitschko, W. *Angew. Chem., Int. Ed.* **2005**, *44*, 6996−7023.
(2) Ma, X.; Whalen, J. B.; Cao, H.; Latturner, S. E. *Chem. Mater.* **2013**, *25*, 3363−3372.
(3) Phelan, W. A.; Menard, M. C.; Kangas, M. J.; McCandless, G. T.; Drake, B. L.; Chan, J. Y. *Chem. Mater.* **2012**, *24*, 409−420.
(4) Massalski, T. B.; Okamoto, H.; Subramanian, P. R.; Kacprzak, L. *Binary Alloy Phase Diagrams,* 2nd ed.; ASM International: Materials Park, OH, 1990; Vol. *1*−3.
(5) Zaikina, J. V.; Zhou, H.; Latturner, S. E. *J. Solid State Chem.* **2010**, *183*, 2987−2994.
(6) Zaikina, J. V.; Zo, Y. J.; Latturner, S. E. *Inorg. Chem.* **2010**, *49*, 2773−2781.
(7) Benbow, E. M.; Dalal, N. S.; Latturner, S. E. *J. Am. Chem. Soc.* **2009**, *131*, 3349−3354.
(8) Tucker, P. C.; Nyffeler, J.; Chen, B.; Ozarowski, A.; Stillwell, R.; Latturner, S. E. *J. Am. Chem. Soc.* **2012**, *134*, 12138−12148.
(9) *SAINT,* Version 6.02a; Bruker AXS, Inc.: Madison, WI, 2000.
(10) Sheldrick, G. M. *SHELXTL NT/2000,* Version 6.1; Bruker AXS, Inc.: Madison,WI, 2000.
(11) Chakoumakos, B. C.; Cao, H.; Ye, F.; Stoica, A. D.; Popovici, M.; Sundaram, M.; Zhou, W.; Hicks, J. S.; Lynn, G. W.; Riedel, R. A. *J. Appl. Crystallogr.* **2011**, *44*, 655.
(12) (a) Koepernik, K.; Eschrig, H. *Phys. Rev. B* **1999**, *59*, 1743−1757. (b) Opahle, I.; Koepernik, K.; Eschrig, H. *Phys. Rev. B* **1999**, *60*, 14035−14041.
(13) Perdew, J. P.; Wang, Y. *Phys. Rev. B* **1992**, *45*, 13244−13249.
(14) (a) Czyzyk, M. T.; Sawatzky, G. A. *Phys. Rev. B* **1994**, *49*, 14211−14228. (b) Eschrig, H.; Koepernik, K.; Chaplygin, I. *J. Solid State Chem.* **2003**, *176*, 482−495.

dx.doi.org/10.1021/ic5005984 | *Inorg. Chem.* 2014, 53, 6141−6148

(15) Anisimov, V. I.; Zaanen, J.; Andersen, O. K. *Phys. Rev. B* **1991**, *44*, 943−954.
(16) Liechtenstein, A. I.; Anisimov, V. I.; Zaanen, J. *Phys. Rev. B* **1995**, *52*, R5467−R5470.
(17) Krier, G.; Jepsen, O.; Burkhardt, A.; Andersen, O. K. *TB-LMTO-ASA Program,* Version 4.7; Max-Planck-Institut für Festkörperforschung: Stuttgart, Germany, 1995.
(18) Jepsen, O.; Andersen, O. K. *Z. Phys. B* **1995**, *97*, 35.
(19) Dronskowski, R.; Blöchl, P. E. *J. Phys. Chem.* **1993**, *97*, 8617.
(20) Cava, R. J.; Takagi, H.; Zandbergen, H. W.; Krajewski, J. J.; Peck, W. F., Jr; Siegrist, T.; Batlogg, B.; Van Dover, R. B.; Felder, R. J.; Mizuhashi, K.; Lee, J. O.; Eisaki, H.; Uchida, S. *Nature* **1994**, *367*, 252−253.
(21) Herbst, J. F.; Croat, J. J.; Pinkerton, F. E.; Yelon, W. B. *Phys. Rev. B* **1984**, *29*, 4176−4178.
(22) Paccard, L.; Paccard, D. *J. Less-Common Met.* **1988**, *136*, 297−301.
(23) Paccard, L.; Paccard, D.; Bertrand, C. *J. Less-Common Met.* **1987**, *135*, L5−L8.
(24) Tang, C.; Fan, S.; Zhu, M. *J. Alloys Compd.* **2000**, *299*, 1−4.
(25) Yelon, W. B.; Hu, Z.; Singleton, E. W.; Hadjipanayis, G. C. *J. Appl. Phys.* **1995**, *78*, 7196−7201.
(26) Garcia, L. B.; Fruchart, D.; Gignoux, D.; Skolozdra, R. V.; Soubeyroux, J. L. *J. Alloys Compd.* **1998**, *278*, 6−16.
(27) (a) Rieger, W.; Nowotny, H.; Benesovsky, F. *Monatsh. Chemie* **1966**, *97*, 378−382. (b) Bronger, W.; Guenther, O. *J. Less-Common Metals* **1972**, *27*, 73−79.
(28) (a) Ballou, R.; Gignoux, D.; Lemaire, R.; Monterroso, R. M.; Schweizer, J. *J. Magn. Magn. Mater.* **1986**, *54*−*57*, 499−500. (b) Zhuang, Y.; Yan, J.; Zhou, H.; Ou, X. *J. Alloys Compd.* **1998**, *266*, 164−166.
(29) Tome, M. A. C. *J. Low Temp. Phys.* **1975**, *20*, 677−689.
(30) Szytula, A.; Leciejewicz, J. *Handbook of Crystal Structures and Magnetic Properties of Rare Earth Intermetallics;* CRC Press, Inc.: Boca Raton, 1994.
(31) (a) Strandberg, T. O.; Canali, C. M.; MacDonald, A. H. *Nat. Mater.* **2007**, *6*, 648−651. (b) Fritsch, D.; Koepernik, K.; Richter, M.; Eschrig, H. *J. Comput. Chem.* **2008**, *29*, 2210−2219.